MIT Libraries | DSpace@MIT

MIT Open Access Articles

Development and characterization of an iodine field emission ion source for FIB applications

The MIT Faculty has made this article openly available. ***Please share*** how this access benefits you. Your story matters.

Citation: Fedkiw, Timothy P., and Paulo C. Lozano. "Development and characterization of an iodine field emission ion source for focused ion beam applications." J. Vac. Sci. Technol. B. AVS, 2009. 2648-2653.

As Published: http://dx.doi.org/10.1116/1.3253604

Publisher: American Vacuum Society

Persistent URL: http://hdl.handle.net/1721.1/60026

Version: Author's final manuscript: final author's manuscript post peer review, without publisher's formatting or copy editing

Terms of use: Attribution-Noncommercial-Share Alike 3.0 Unported

Massachusetts Institute of Technology

Development and characterization of an iodine field emission ion source for FIB applications

Running title: Iodine ion source for FIB applications

Running Authors: Fedkiw and Lozano

Timothy P. Fedkiw[a)]

and Paulo C. Lozano

Department of Aeronautics and Astronautics, Massachusetts Institute of Technology, Cambridge, MA 02139

[a)]Electronic mail: tpfedkiw@mit.edu

Emission of positive and negative ions is possible when a room temperature molten salt, or ionic liquid, is exposed to a sufficiently high electric field. Ionic liquid ion sources (ILIS) have shown potential to be used in various focused ion beam (FIB) applications, since their operation and characteristics are similar to those of liquid metal ion sources, with the advantage that ILIS work at low temperatures in comparison and a large number of ionic liquids with many different compositions are available. In this paper we present results on the emission characteristics of negative ions extracted from an iodine-based ionic liquid using a time-of-flight mass spectrometer and a retarding potential analyzer. The ionic liquid BMI-I is used as source media, producing a droplet free beam with multiple solvated ion species. Attention is given to BMI-I in particular due to the potential of creating a beam of pure and clustered I- ions, which are expected to improve the performance in applications based on secondary emission and reactive species. Properties important to the focusing of the ion beam such as mass and energy distributions are obtained. Effects on the ion emission are studied through a comparison of the source using temperature as a parameter to modify the liquid viscosity and electrical conductivity.

I. INTRODUCTION

Ionic liquids, also known as room-temperature molten salts, are unique substances that have recently found applicability in a wide number of industrial processes and

devices, most of them in the chemical industry as media for catalysis and synthesis[1], but also as electrolytes for supercapacitors[2] and as space propulsion propellants[3]. Ionic liquids are composed of a wide variety of complex organic and inorganic cations (C+) and anions (A-). Since there is no solvent in these liquids, particle-particle interactions are coulombic in nature, and therefore much stronger than typical van der Waals forces. As a consequence, these liquids have non-measurable vapor pressures at moderate temperatures, which allows for operation under high vacuum. Ionic liquids have also relatively high electric conductivities and are therefore susceptible to hydrodynamic electrospraying. A team led by F. de la Mora discovered[4] that at low flow rates, an initially droplet-rich regime transitions into a purely ionic regime, a unique situation not encountered with any conventional electrolytic solution. However, this observation was only valid for the popular ionic liquid EMI-BF_4 when electrospraying from capillary emitters.

Since then, ionic liquid ion sources (ILISs) have been shown to be a reliable source for high brightness and monoenergetic ion beams composed of either positive or negative ions[5,6,7]. Similarly to LMIS, an ionic liquid layer coats a sharp tungsten needle from which positive and negative ions are field evaporated. An electric field strength on the order of a few volts per nm is required to trigger ion evaporation from most ionic liquids. Fields of this magnitude are easily achievable near the apex of dynamically-stable Taylor cones[8]. Recent studies have shown that a wide variety of ions can be obtained using different ionic liquids with the ILIS configuration. Table 1 shows a list of ionic liquids which have been used in ILIS sources, all of them producing a stream of positive or negative solvated ions of the type $(CA)_nC+$ and $(CA)_nA-$, depending on the applied polarity. The degree of solvation n is typically evenly distributed (by current) between $n = 0$ and $n = 1$ ions, with smaller traces of larger species.

Several of the ionic liquids studied have been seen to produce high brightness and nearly monochromatic ion beams, similar to those produced by LMIS[9]. This has led to the investigation of the use of ILIS in FIB applications[13]. In a FIB system, the ultimate goal is to focus the ion current into the smallest possible area. A common way of estimating the probe size, d, for an ion optical system[14] is

$$d^2 = I^3 \frac{C_s^2}{\left[\pi M^2 \left(\frac{dI}{d\Omega}\right)^3\right]} I\left(\frac{\Delta W_{1/2}}{W}\right)^2 + \frac{C_c^2}{\pi M^2 \left(\frac{dI}{d\Omega}\right)} M^2 D^2 \quad (1)$$

Where I is the beam current, $dI/d\Omega$ is the angular brightness, $\Delta W_{1/2}$ is the energy spread (FWHM) of the beam, W is the energy, and D is the source size. The other parameters are the spherical and chromatic aberration coefficients, C_s and C_c respectively, and the magnification, M, all of which are dependent on the optics of the system, not on the ion source itself. Therefore, the important parameters to characterize an ILIS for use in FIB are the energy spread, source size, brightness, and operating currents. It is well acknowledged that chromatic aberration tends to be the mechanism that limits the resolution of LMIS. Since the operating principles are similar, it is expected that an equivalent situation should occur in ILIS, except for the basic but important difference that ILIS operate with significantly lower currents (typically between 10 and 1000 nA). This property results from the combination of lower surface tension and much lower electrical conductivity of ionic liquids in comparison to liquid metals. It is therefore important to characterize the energy dispersion of ILIS beams, in order to obtain limits on beam focusing in the low current regime.

All of the ILIS studies up to this point have produced molecular ions, but there are several ionic liquids that have monatomic anions, in particular halogen species, such as BMI-I, EMI-I, BMI-Cl, EMI-Cl among others including fluorine and bromine ions. For this paper, we will focus on the liquid BMI-I, 1-ethyl-3-methylimidazolium iodide. Table 2 contains a list of the properties of this ionic liquid. The conductivity of the liquid is not well defined in the literature, so it had to be determined experimentally. A container of BMI-I was placed in a hot water bath to control the temperature, and an electric conductivity meter was used to measure the conductivity. All other properties were obtained from literature[15]. It is interesting to note that ion emission is possible from this liquid, despite its low conductivity and exceptionally high viscosity as compared to other liquids in Table 1. The attractiveness of this ionic liquid lies in its ability to produce a beam of monatomic negative iodine ions that would allow for the combination of chemical reactivity, enhanced sputtering rates and increased secondary emission in FIB

applications, an application that iodine ions have already been used for using a plasma source.

II. EXPERIMENTAL PROCEDURES

The ionic liquid BMI-I was synthesized in-house using the process described in Ref. 15. In short, the synthesis involves three steps of (1) combining equimolar amounts of idobutane and 1-methylimidazole and allow to react for 72 hours, (2) cleaning the resulting liquid with ethyl acetate, (3) removing the ethyl acetate using a vacuum line.

The ILIS emitter is prepared from a 0.5 mm DIA tungsten needle that undergoes a treatment to encourage flow to the tip. The treatment, described in detail in Ref. 5, involves an electrochemical etch, followed by an annealing process and microroughing in a potassium ferrocyanide solution. As shown in Fig. 1, the emitter tip is centered in the entrance plane of an extractor of 1.5 mm diameter. A chamber a few millimeters prior to the tip holds a supply of the ionic liquid, and a heating element attached to the needle allows for temperature control. The emitter is connected to a bipolar high voltage power supply, and can be set to a potential (V_{app}) relative to the electrically grounded extractor. The emitter is wetted with ionic liquid and placed in a vacuum chamber at a pressure of approximately 1 x 10^{-6} Torr, and is operated at a temperature of approximately 50 °C. Even though ion emission is possible at room temperature using BMI-I[17], it was found that the increase in conductivity and decrease of viscosity at 50 °C resulted in much more stable emission. The source module is mounted on a flange, to which instruments can be attached in order to ensure proper alignment. For this study, the beam composition was determined using a wide-dynamic range time-of-flight mass spectrometer, and the energy properties were measured using a retarding potential analyzer (RPA).

A. Time-of-flight mass spectrometer

The design of the TOF spectrometer is nearly identical to that from Ref. 9 and is shown in Fig. 1a. A 3-element einzel lens is mounted approximately 8.8 mm away from the extractor with the outer electrodes grounded and the inner electrode set at a focusing voltage V_f. The lens serves to collimate the beam in order to prevent signal spreading from angular divergence, as well as to intensify the signal at the detector and increase the resolution by allowing a longer drift distance. Immediately following the third lens

electrode is an electrostatic interleaved-comb gate, composed of 0.127 mm tungsten wires spaced by 1.2 mm, and connected to a ±900 V pulse amplifier driven by a pulse generator. A metal plate 38 mm in diameter is located approximately 760 mm (distance-of-flight, L) from the gate to serve as a detector. This collector plate is connected to an oscilloscope through a wide-band current amplifier. Two tungsten grids are located 2.5 mm from the detector. The outermost is grounded, while the other is biased to -30 V to suppress secondary electron emission.

B. Retarding potential analyzer

For the retarding potential analyzer, the einzel lens is again mounted about 8.8 mm from the extractor. The purpose of the lens is to obtain a collimated ion beam and therefore remove the energy spectra broadening due to beam divergence. Following the third electrode is a grounded aperture and a shielded drift region of about 12 mm, with the actual RPA at the end of this drift region. The RPA constructed for this study is a combination of two designs as shown in Fig. 1b. The basic form of the instrument is taken from Ref. 18. A metallic cylinder of 25 mm diameter and 25 mm length is placed within a grounded enclosure with a small entrance aperture (3 mm diameter). At one end of the cylinder is a mesh, followed by the collector plate. In order to prevent potential sagging, two additional grids were placed at the end of the cylinder and one at the entrance aperture. This design choice was made based on Ref. 19, which proved that multiple grids could be used to create deep equipotential regions. All grids are composed of 76 μm diameter tungsten wires, with spacing of 0.76 mm, giving a 90% transparency for each grid. The distance between grids at the end of the cylinder is 0.65 mm. The collector used in this RPA is a Faraday cup connected to an oscilloscope through a high impedance electrometer. A high voltage triangular wave is applied to the RPA at very low frequencies (period of 30 seconds). Post processing of the collected signal involves low-pass filtering to eliminate noise, followed by a second-order finite difference scheme to obtain the energy distribution.

In addition to the configuration shown in Fig. 1b, the RPA is also operated without the einzel lens in order to obtain an energy spectrum of the unfocused ion beam. For this operation, the entrance to the RPA is placed 6.3 mm from the exit plane of the

extractor. While operating in this configuration causes an apparent broadening of the energy spectrum, it allows for a snapshot of the entire beam within a given solid angle, rather than of a certain energy range selected by the einzel lens.

III. RESULTS AND DISCUSSION

As for other ionic liquids, the BMI-I based ILIS can be operated in either positive or negative polarity. Operation in dc mode would result on the accumulation of counter-ions on the liquid-needle interface, eventually leading to electrochemical reactions. It has been shown that this situation can be avoided by operating the source in alternating mode with a polarity reversal frequency of 1 Hz or less[5]. In some instances, mostly when operating the source in the positive mode thus accumulating negative ions, the products of electrochemical decay accumulate and degrade the liquid and the ILIS operation. However, most positive ions of ionic liquids (EMI, BMI, C_6MI and others) are released as gas when discharged, thus allowing operation of an ILIS source based on these ions for long times without damage to the liquid or the needle emitter. Since the focus of this paper is on the development of an iodine ion source, only the negative mode of operation in dc mode has been considered.

A. Beam Composition

In order to identify the masses of the charged particles emitted from the ILIS, the TOF current signal is transformed by using conservation of energy to obtain

$$\frac{m}{q} = \frac{2V_{acc}t^2}{L^2} \quad (2)$$

where L is the drift region length, t is the time to travel this distance, and V_{acc} is the voltage through which the particle has been accelerated. The value of this accelerating voltage will be less than the voltage applied to the emitter, V_{app}. This deficit, D, can be attributed the work required to bring an atom or molecule from the liquid to the gas phase, along with other losses[6]. It is assumed that all charged particles that are present in the beam are singly charged, and the conversion given by Eq. (2) is performed, followed by a second-order finite difference scheme to obtain the mass spectrum.

Similar to prior studies of ILIS, the charged species contained in the beam are found to be composed of an ion attached to a number of neutrals, being of the form

$(BMI\text{-}I)_nI^-$. The ion beam is composed of three distinct species, with degrees of solvation $n = 0, 1, 2$. Fig. 2a shows the resulting mass spectrum for an applied voltage of -1500 V. There are two distinct peaks that correspond to the ions I^- and $(BMI\text{-}I)I^-$. Although it cannot be seen in the spectrum, by looking directly at the current signal in Fig. 2b it is seen that the doubly solvated ion $(BMI\text{-}I)_2I^-$ is also present, although in a much smaller amount. Descriptions of the different ionic species observed are given in Table 3. Only these ionic species were observed, with no indication of charged droplets at longer flight times (up to several ms). Nearly half of the collected signal is seen to be due to negative iodine ions, with the rest being composed of the singly solvated species.

B. Energy Distribution

Fig. 3 shows the energy distribution for applied potentials of -1500, -1600, and -1700 V. Each spectrum contains a strong, sharp peak slightly below the applied potential, with a full with at half maximum (FWHM) of approximately 10 eV. The energy deficit, *D*, is seen to be approximately 10-15 eV in all cases. In addition to the primary peaks, each of these spectra also contains secondary signals of lower intensity, which are difficult to observe in the figure. The implications of these signals will be discussed in further detail in the next section. In the current configuration, no provision is made to select one of the different species detected in the beam. This means that the energy distribution observed contains all charged species. From an energy standpoint alone, it could be expected that the energy of solvation, here defined as the energy required to extract an ion from the liquid surface, would be different for ions with different degrees of solvation. It is possible then that even narrower energy distributions would result if indeed two superimposed signals corresponding to each ion family are represented by the sharp signal observed in the figure. Further work is required in this direction, nevertheless, these results serve to illustrate that it is possible to obtain negative iodine ion beams with relatively narrow energy distributions from this ILIS, making it adequate for use in a FIB column.

C. Ion Fragmentation

As mentioned in the previous section, there are several secondary features present in the energy spectrum of the emitted ion beam. These secondary signals can be

attributed to the fragmentation of some charged particles before reaching the detector. The action of an electrostatic lens depends only on the emission potential of the charged particles, not their specific charge. This means that the energy distributions shown in section B are primarily for a specific range of energies close to the position of the main peak. In order to obtain a better idea of the total beam energy distribution, the RPA analysis was performed a second time with the einzel lens removed, at the expense of lower resolution due to beam divergence, resulting in the energy distribution shown in Fig. 4. Again the most prominent peak appears just below the applied potential, but there are two smaller peaks. In order to understand the meaning of this secondary signal, consider a singly charged ion of degree of solvation n, accelerated through a potential V_{acc}. The total kinetic energy, K, of the ion will be given by qV_{acc}. If this ion fragments into a neutral and a smaller ion (degree of solvation $m < n$), the final kinetic energy of the ion will be

$$K_{n\rightarrow m} = \frac{m_m}{m_n}\left|qV_{acc}\right| \qquad (3),$$

assuming that breakup occurs in a region of zero potential. This means the stopping voltage in the RPA will be decreased by a factor given by the ratio of masses. Table 4 lists the stopping voltages (normalized to the accelerating voltage) for a variety of ion fragmentation of $(BMI\text{-}I)_nI^-$ into $(BMI\text{-}I)_mI^-$. The signal from the RPA shows significant breakup of $1\rightarrow 0$ and $2\rightarrow 1$. However, an interesting feature that cannot be seen in the spectrum is shown in the current signal in Fig. 5. In addition to the steps that indicate the primary signal and ion breakup, there is a more or less constant slope contained between the first and last steps. In previous studies using capillary emitters, such broad spreads at lower energies have been associated with the presence of charged droplets in the beam. However, the sharply defined primary and secondary steps exactly at the corresponding potentials predicted by ion fragmentation, and the lack of a droplet signal in the TOF-MS measurements rules out their presence. This leads to the conclusion that solvated ions are metastable, and breakup is occurring in significant amounts in regions with a potential not equal to zero. The continuous nature of the potential drop between secondary peaks suggests that solvated species break up promptly upon emission while still inside the emitter-extractor acceleration region. Molecular dynamics simulations of the emission

process with EMI-BF_4 show that prompt fragmentation is indeed possible[20] and is therefore a plausible explanation of the observed spectra.

IV. CONCLUSIONS

Emission of ions of the form $(EMI\text{-}I)_nI^-$ (n = 0,1,2) from a tungsten needle externally coated with EMI-I has been demonstrated. The TOF-MS measurements confirm the presence of three ionic species, and the absence of charged droplets. The energy properties of this iodine ILIS were studied using an RPA, displaying a narrow (~10eV) main peak, but with a significant secondary signal. This secondary signal is likely due to ion breakup in regions of nonzero potential. However, the production of an ion beam with a large portion of pure iodine ions of a low energy spread makes this ILIS an attractive ion source for FIB applications. In a practical arrangement, energy and mass filtering would be required. Also, a more detailed investigation of the breakup process is needed, in particular measuring the spatial-temporal fragmentation distributions would yield important information on the stability of solvated ions, their internal energies and their emission mechanics.

Acknowledgements

T. Fedkiw would like to thank the MIT Department of Aeronautics and Astronautics for financial support for this study. We would like to thank Enrique Citron for his work in the synthesis of the BMI-I used for this study.

[1]T. Welton, Chem. Rev. **99**, 2071 (1999).

[2]M. Ue, M. Takeda, A. Toriumi, A. Kominato, R. Hagiwara, and Y. Ito, J. Electrochem. Soc. **150**, A499 (2003).

[3]M. Gamero-Castaño, V. Hruby, J. Propulsion Power **17**, 977 (2001).

[4]I. Romero, R. Bocanegra, J. Fernandez de la Mora, and M. Gamero-Castano, J. Appl. Phys. **94**, 3599 (2003).

[5]P. Lozano and M. Martinez-Sanchez, J. Colloid Interface Sci. **280**, 149 (2004).

[6]P. Lozano and M. Martinez-Sanchez, J. Colloid Interface Sci. **282**, 415 (2005).

[7]S. Castro and J. Fernandez de la Mora, J. Appl. Phys. **105**, 034903 (2009).

[8]G. I. Taylor, Proc. R. Soc. London **383**, 383 (1964).

[9]P. Lozano, J. Phys. D **39**, 126 (2006).

[10]C. Larriba, S. Castro, J. Fernandez de la Mora, and P. Lozano, J. Appl. Phys. **101**, 084303 (2007).

[11]S. Castro, C. Larriba, J. Fernandez de la Mora, P. Lozano, S. Sümer, Y. Yoshida, G. Saito, J. Appl. Phys. **102**, 094310 (2007).

[12]N. Takahashi, A. N. Zorzos, and P. C. Lozano, in *Proceedings of the 2008 Joint Symposium on Molten Salts*, Molton Salt Committee, The Electrochemical Society of Japan, p. 599 (2008).

[13]A. Zorzos and P. Lozano, J. Vac. Sci. Technol. B, **26**, 2097 (2008).

[14]J. Orloff, L. Swanson, and M. Utlaut, *High Resolution Focused Ion Beams: FIB and Applications* (Springer, New York, 2002).

[15]J. G. Huddleston, A. E. Visser, W. M. Reichert, H. D. Willauer, G. A. Broker and R. D. Rogers, Green Chem. **3**, 156 (2001).

[16]J. Zhou, W. Ens, K.G. Standing, Int. J. of Mass Spect. And Ion Proc. **146**, 139 (1995).

[17]A. Zorzos. SM Thesis, MIT, June 2009.

[18]Y. Zou *et al.*, Phys. Rev. ST Accel. Beams **5**, 072801 (2002).

[19]C. L. Enloe and J. R. Shell, Rev. Sci Instrum. **63**, 1788 (1992).

[20]N. Takahashi and P. Lozano, "Computational Investigation of Molecular Ion Evaporation in Electrospray Thruster," *The 44th Joint Propulsion Conference and Exhibit*, Hartford, CT, 2008

Table 1: Ionic liquids with verified ion emission
Table 2: Properties of BMI-I
Table 3: Ionic species observed in the TOF-MS
Table 4: Stopping voltages for breakup of negative ions

FIG 1. Experimental setup for the (a) time of flight mass spectrometer and (b) the retarding potential analyzer.

FIG 2. TOF-MS measurement with applied voltage of -1500V. (a) Plot of the mass spectrum and (b) of the collected current.

FIG 3. RPA energy spectra results for applied voltages of -1.5, -1.6, -1.7 kV.

FIG 4. RPA energy spectrum for the full beam at -1.5kV

FIG 5. Current collected by the RPA for the full beam at -1.5kV

Table 1

Ionic Liquid	Ref.
EMI-BF_4	4
EMI-Im	9
BMI-$FeBr_4$	10
EMI-$GaCl_4$	10
EMI-$N(CN)_2$	10
C_6MI-$FeBr_4$	10
C_6MI-$FeCl_4$	10
C_5MI-$(C_2F_5)_3PF_3$	11
EMI-Beti	11
EMI-F2.3HF	12

Table 2

Surface Tension	0.0547 N/m
Density	1440 kg/m3
Viscosity	1110 cP (25 C)
	~500 cP (estimated for 50 C)
Conductivity	0.069 S/m (23 C)
	0.25 S/m (50 C)
	0.73 S/m (75 C)
BMI Mass	139.2 g/mol
Iodine Mass	126.9 g/mol

Table 3

Ion Observed	Ion mass (Da)	Time of flight (μs)
I^-	126.9	15.4
$(EMI\text{-}I)I^-$	392.8	26.9
$(EMI\text{-}I)_2I^-$	658.7	35.0

Table 4

Initial → Final degree of solvation	V_{stop}/V_{acc}	V_{stop} for V_{acc} = -1490V
1 → 0	0.32	-477V
2 → 1	0.60	-894V
2 → 0	0.19	-283V

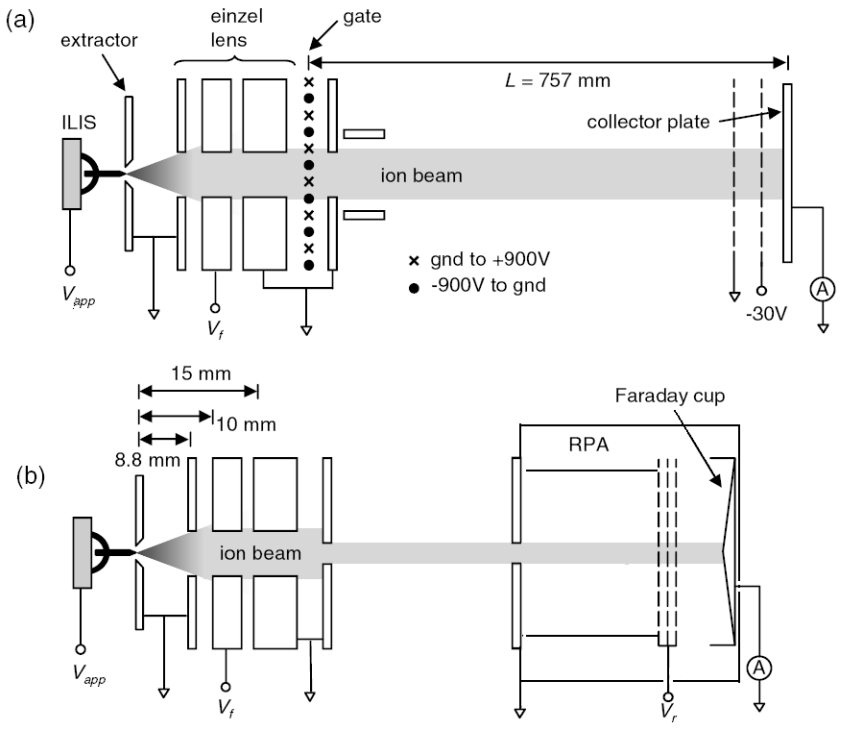
(a)
extractor
einzel lens
gate
L = 757 mm
ILIS
collector plate
ion beam
gnd to +900V
-900V to gnd
-30V
A
(b)
15 mm
10 mm
8.8 mm
Faraday cup
RPA
ion beam
A

FIG 1.

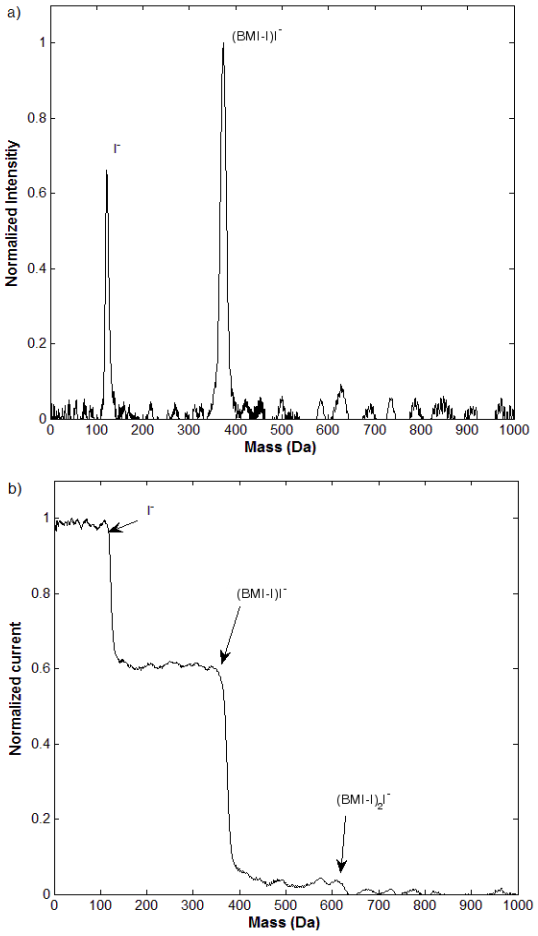
a)
(BMI-I)I⁻
I⁻
Normalized Intensitiy
Mass (Da)
b)
I⁻
(BMI-I)I⁻
(BMI-I)2I⁻
Normalized current
Mass (Da)

FIG 2.

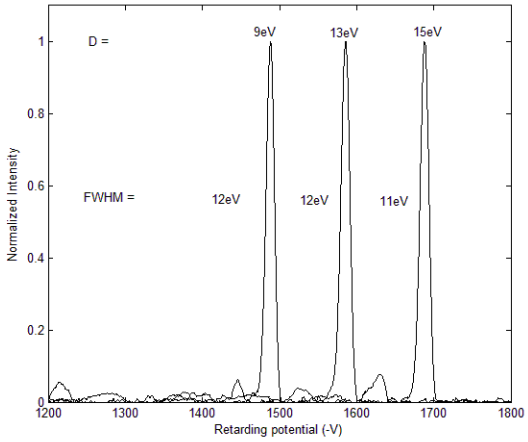
D =
9eV
13eV
15eV
FWHM =
12eV
12eV
11eV
Normalized Intensity
Retarding potential (-V)
0
0.2
0.4
0.6
0.8
1
1200
1300
1400
1500
1600
1700
1800

FIG 3.

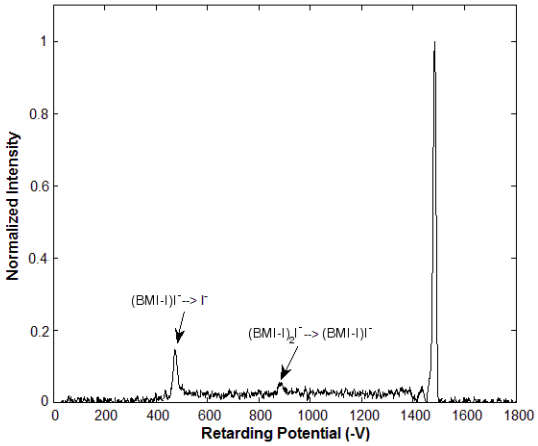
Normalized Intensity
Retarding Potential (-V)
(BMI-I)I⁻ --> I⁻
(BMI-I)2I⁻ --> (BMI-I)I⁻
0
0.2
0.4
0.6
0.8
1
0
200
400
600
800
1000
1200
1400
1600
1800

FIG 4.

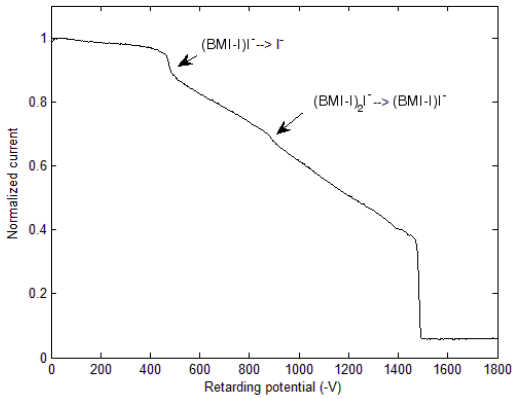
(BMI-I)I⁻--> I⁻
(BMI-I)2I⁻--> (BMI-I)I⁻
Normalized current
Retarding potential (-V)
0
0.2
0.4
0.6
0.8
1
0
200
400
600
800
1000
1200
1400
1600
1800

FIG 5.